JOURNAL OF MECHANICS OF CONTINUA AND MATHEMATICAL SCIENCES
www.journalimcms.org

ISSN (Online) : 2454 -7190 Vol.-18, No.-12, December (2023) pp 32-46 ISSN (Print) 0973-8975

PERFORMANCE ANALYSIS OF OPTICAL PARALLEL FULL ADDER USING ARTIFICIAL NEURAL NETWORK

Arunava Bhattacharyya[1], Asish Mitra[2]

[1]Asso. Prof., Department of Information Technology & Computer Science, College of Engineering & Management, Kolaghat, India

[2]Prof. Department of Basic Sciences, College of Engineering & Management, Kolaghat, WB, India

Email : arunava_bhatt@yahoo.com[1], asish@cemk.ac.in[2]

Corresponding Author: **Asish Mitra**

https://doi.org/10.26782/jmcms.2023.12.00003

(Received: October 07, 2023; Revised: November 27, 2023; Accepted: December 02, 2023)

Abstract

A verbal exchange today wishes for quick operational progress. This can be accomplished by replacing devices that are primarily concerned with commutation and logic with photon-based systems instead of the usual data service, the electron. The basic building blocks of superior frames are called gates. With the aid of these gates, various logical and mathematical operations can be performed. All-optical arithmetical and logical processes are eagerly expected in high-speed dialogue frameworks. In this chapter, we've introduced parallel models for adding two binary digits that are based on Sagnac gates with help from semiconductor optical amplifiers (SOA) and terahertz optical asymmetric demultiplexers (TOAD). We created a Full adder that works in parallel using only two TOADs as total switches. Using artificial neural networks (ANN), we have created a model of this circuit that is equivalent. Utilizing ANN, this circuit design has been validated. This optical circuit is now capable of synthesizing light as an input and successfully structuring the aspiration output in addition to speeding up calculation. This parallel circuit's biggest advantage is that it doesn't need synchronization for distinct inputs. An ANN model was used to analyze this circuit's performance in detail.

Keywords: artificial neural networks, optical logic, semiconductor optical amplifier, Terahertz optical asymmetric demultiplexer.

I. Introduction

Modern high-speed all-optical presence-of-mind entryways are crucial components in optical organizations because optical processing works the fundamental sign-handling features, such as exchanging recovery and mindfulness handling, on photonic exchanging hubs [XIX, VI, XI]. The entire method for managing optical records has been rendered useless. The Sagnac Gate with Terehartz Optical Asymmetric Demultiplexer (TOAD)/Semiconductor Optical Amplifier (SOA) is one of the many optical switches that successfully combines low strength

usage, excessive repetition cost, and quick exchanging time [I, XVI, XVII]. Through certain query organizations, half-viper using the SOA-aided Sagnac interferometer has been proposed and demonstrated [XX, XII, II, XXIII, XVIII]. A modern approach to using optical recurrence-encoded tasks that makes use of the Mach-Zehnder interferometer was developed by Ghosh et al [XXI]. Recent developments in neural networks have been quite exciting. stages of elective computing. Neural networks are developing theories to remove barriers to increased computational efficiency. A potential solution to the energy-cost problem that deep learning is trying to solve is provided by optical neural networks [XXIV]. In order to understand an optical lattice duplication unit that is completely inactive for neural network applications, straight optics have been used in free-space optical circuits [XXV]. Machine learning (ML) has advanced all researchers studying the interaction of light and matter, with the aid of advances in materials science, physical science, and photonics. The first is the development of intelligent photonic frameworks, and the second is the integration of machine learning (ML) into physical and chemical sciences for comprehensive information security and creative primary experiences [XIII]. X. Wu et al. present a method for optical execution testing of quadrature stage shift-keying information signals that makes use of fake brain networks built with boundaries taken from unconventional charts. Additionally, authors show that nonconcurrent outlines built from modified locations produce better results when compared to single-finished identification in 100 Gb/s. The exploratory show attests to the suitability of the suggested course of action [XXVI]. The authors demonstrate how a nuclear fume cell can perform a close nonlinear actuation in two ways, enabling the execution of a fully optical ANN for the recognition of manually written digits in images. Such a company is capable of handling a lot of information simultaneously [III]. Large-area optical switches, which have the crucial benefits of low power consumption and short idle time, are necessary for facilitating the ever-increasing exchange of information with one another more and more frequently in intra- and inter-datacenter contexts. Coordinated silicon photonics has recently demonstrated exceptional promise for creating large-scale optical switch textures for usage in cutting-edge all-optical networks due to the benefits of minimal imprint and quick response time [XXVII]. An optical beneficiary for binaries is suggested by the authors. The opto-electronic components are used in this optical neural network. This network has a variety of layers. Three layers are used in this. The transmission layer is the top layer, followed by the optical neuron layer and the electronic neuron layer. The information optical sign is copied and chosen for transmission into the opto-electronic network by the transmission layer, which is based on the Mach-Zehnder interferometer (MZI). The transmission layer and optical layer, both of which can be built on the silicon layer, which was created especially for the planning of binarized loads into optical space [28]. In this chapter, we were familiar with two-digit work growth in equal styles, mostly focused on Sagnac entryways based on (TOAD). We have only planned to use two TOADs-based switches for the parallel half-adder. We have designed an ANN-based model of this circuit that is equivalent. Utilizing ANN, this circuit setup has been verified. This optical circuit is now capable of successfully arranging light as an input to shape the aim, in addition to increasing calculation speed. The biggest benefit of this parallel circuit is that no synchronization for unique data sources is

anticipated. This circuit's subtleties execution examination is finished by the ANN model.

II. Architecture of Switch

A TOAD-based switch's [XIV, V, VII, VIII, IX, X] basic design is shown in Figure 1. In this picture, an irregular component is organized in an uneven circle. The optical enhancer made of semiconductors is employed. In this chapter, we tried to use the results from both the transmitting and reflecting modes:

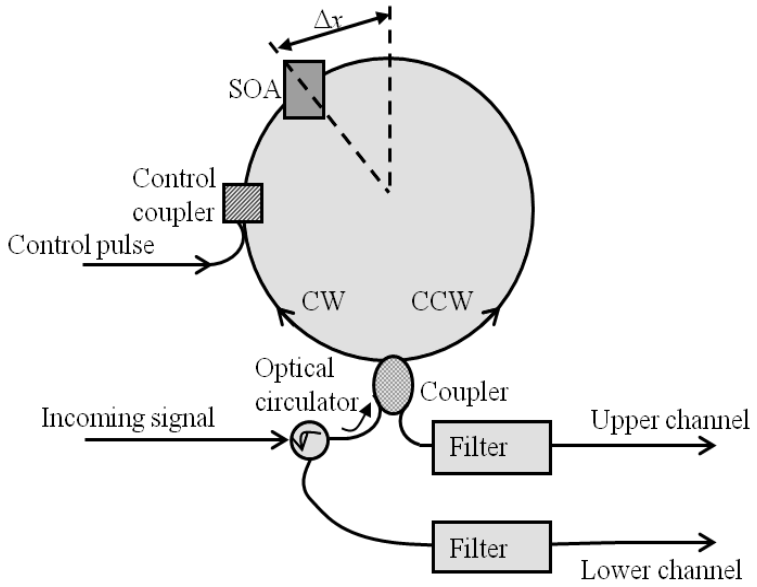

Fig. 1. Basic structure of TOAD.

The power of transmitting (POW_{Up}) and reflecting (POW_{Low}) port might be expressed as [XIV, V, VII, VIII, IX, X]

$$POW_{Up}(t) = \frac{POW_{in}(t)}{4} \cdot \left\{GAIN_{cw}(t) + GAIN_{ccw}(t) - 2\sqrt{GAIN_{cw}(t) \cdot GAIN_{ccw}(t)} \cdot \cos(\Delta\emptyset)\right\} \quad (1)$$

$$POW_{Low}(t) = \frac{POW_{in}(t)}{4} \cdot \left\{GAIN_{cw}(t) + GAIN_{ccw}(t) + 2\sqrt{GAIN_{cw}(t) \cdot GAIN_{ccw}(t)} \cdot \cos(\Delta\emptyset)\right\} \quad (2)$$

Here gain in a clockwise direction is $GAIN_{cw}$ and gain in counter clockwise direction is $GAIN_{ccw}$(Phase difference between these two gains is = –β/2 $\log_e$ $(GAIN_{cw}(t)/GAIN_{ccw}($. The line-width improvement factor is β.

In the absence of a control (CP), the incoming signal enters the circular system via the optical circulator. The loop receives this signal after it has been divided into two parts. While one half rotates anticlockwise, the other rotates in the reverse direction.

Unsaturated gain is the same for both signals. The two signals acquire the same gain when they recombine at the input, i.e. at that time, the phase difference between these is almost equivalent to zero, i.e. When this happens, the gain in the upper port is almost equal to zero, i.e. Thus, where is the modest signal gain, the gain in the lower port is. The source of the information appears to be mirrored. When using a CP, after it enters the system and modifies the SOA's attributes. The appeal of SOA is fading quickly. Both signals exhibit varying degrees of unsaturated gain. The two signals obtain a different gain when they recombine at the input, i.e. The phase difference between them at that moment is approximately equal to 1, or. When this happens, the upper port gain is almost equal to but still not zero. The power in the lower port, however, is essentially zero, so. As a result, the information is currently only visible in the upper port. The power at the upper port can be calculated using equation (1). Similarly, equation (2) can be used to determine the power at the lower port. It is possible to use a band pass filter at the output ports. This filter allows the incoming signal to pass through while blocking the control signal. Figure 2 displays an equivalent drawing of a TOAD.

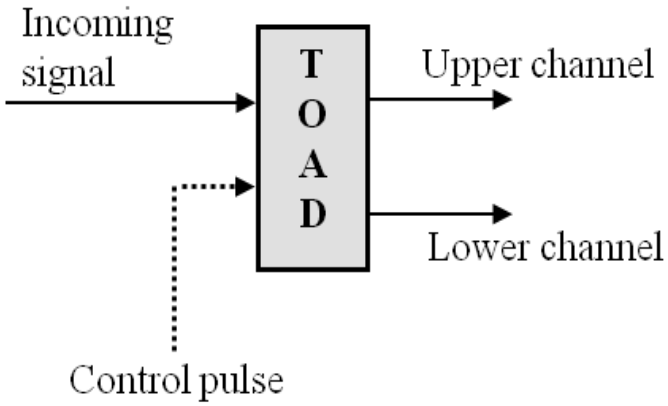

Fig. 2. The drawing of TOAD.

III. Optical Logic-Based Parallel Full Adder

Three numbers namely A, B, and C all are binary one-bit numbers, are added using a circuit based on parallel full adder logic and it will give the result of, a sum (s) and a carry (Cout) of two one-bit binary numbers. The principle of operation of optical logic-based full-adder parallel is illustrated in Fig. 3. Five switches based on TOAD, namely T1 to T5 are used to logically design the adder circuit.

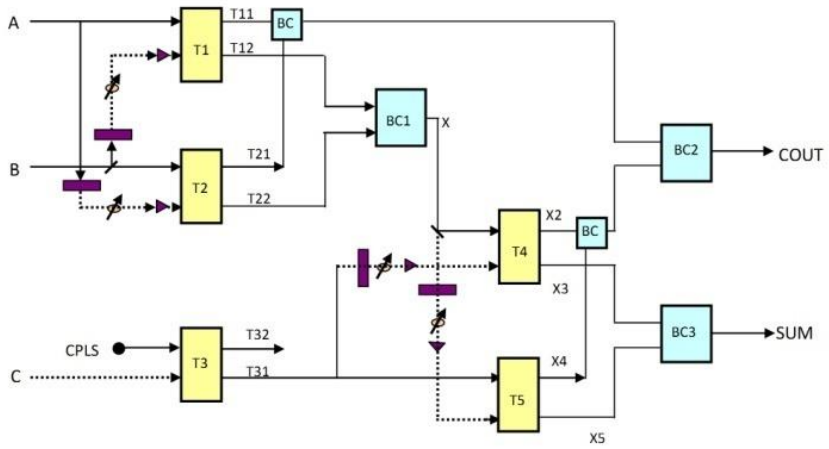

Fig. 3. Diagram of parallel Full adder, where A and B: Inputs, BC: Beam combiner, /: Beam splitter, and Sum and Cout: Final outputs.

The wavelength of the input signal can be appropriately adjusted by the wavelength converter, allowing the same input to be used in this circuit as both a control and an incoming signal. The output is acquired based on the input variables state (A, B, and C) and the corresponding outcome is get from BC2 for Carry Out and BC3 for Summation. The inputs are no longer required for synchronization in this parallel adder circuit.

IV. Optical Neural Network

Optical neuron networks (ONN) emerge as circumstances demand. It is a promising approach to replace fake brain structure because it has the properties of high transmission capacity, high connectivity, and interior equal handling, which can speed up the midway activity of programming and electronic equipment, even up to "light speed." Lattice expansion is possible in a photonic structure at the speed of light, which can effectively resolve the thick grid expansion in the artificial brain organization and save energy and time consumption. Nonlinear optical components may also be used to recognize the nonlinearity in ANN. The entire construction can do the optical sign computation without requiring any extra energy input once the optical brain network's setup is complete. ANN defeats the constraints of conventional methods nowadays. An ANN is set up without the use of a specific condition structure, but good knowledge and yield data are essential. After being regularly trained, an ANN estimate may adapt to new data. When configured correctly, an ANN can examine the information yield's data to learn any straight or nonlinear link. The input level is the first level of this neural network, the output level is the last, and the intermediate level is the hidden level, as shown in Figure 4. One TOAD is used to represent this Figure. In this scheme, the input layer is made up of seven neurons in particular. According to the framework's contributions, the loop eccentricity is represented by the contributions of the incoming pulse (Pin(t)), the width of the incoming pulse (τ_0), recovery of gain time of the SOA (τ_e), loop energy (Pcp(t)),

control pulse energy (E_{cp}), and control pulse width (σ). Two neurons, specifically the upper channel (PUpper) and lower channel (PLower), make up the outcome layer. The test dataset, the training dataset, and the validation dataset are the three segments of our dataset. Multiple datasets are utilized for a variety of aims. Using the training dataset, we were able to manipulate how the neurons were organized.

The organization modifies its weight capacity to reduce inaccuracy. The validation dataset determines whether network hypotheses perform better than that, and we have completed our preparation. With the aid of The organization's performance is assessed both before and after testing using the testing dataset. In this approach, 85% of the total data collection is used for the preparation cycle, 10% is used for testing, and the remaining dataset is used to evaluate network execution.

We used 18 neurons from the buried layer for this technique. The common squared divergence between results and targets is known as the mean square error (MSE). Small gestures are preferable. This value, you may be certain, is zero. The range of MSE for producing, approving, and testing datasets with numerous epochs is shown in Figure 5. The figure demonstrates that for period 22, 0.099065 is the optimum approval execution. When attention error amounts approach epoch 22 and keeps rising, we must stop.

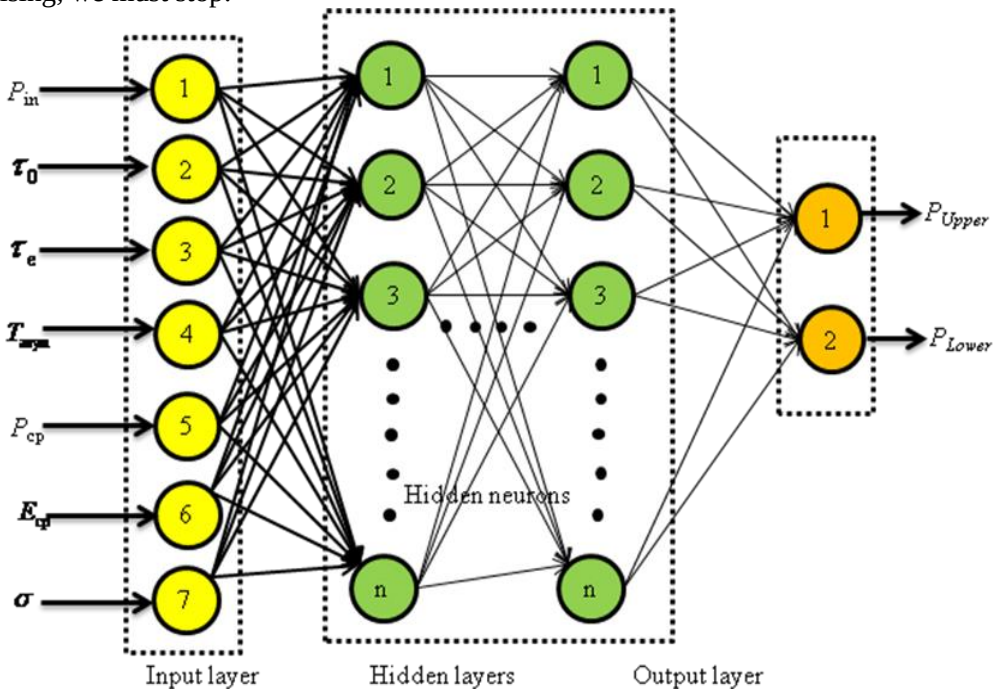

Fig. 4. An artificial neural network with a single TOAD has an input level with seven neurons and an output level with two neurons as its structural components.

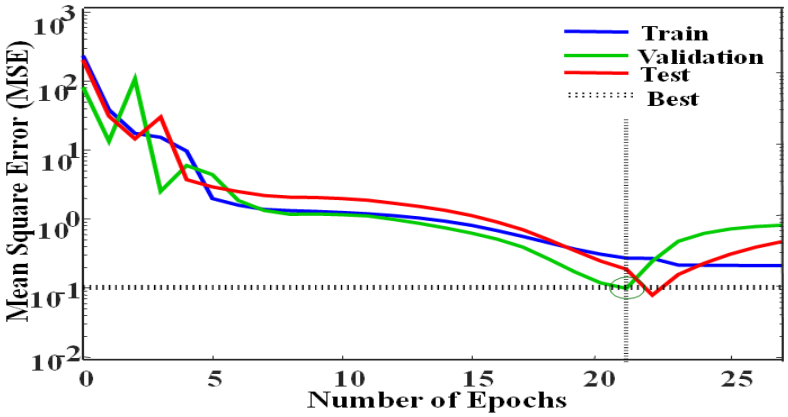

Fig. 5. Change of MSE concerning the number of epochs for the validation, training, and testing data sets.

The correlation between results and goals determines the significance of a direct relapse. Close relationships always have a value of 1 and 0. Figure 6 displays the informative collection's relapse. (Building, endorsing, verifying, and generally). As can be observed from the photos, the relapse factor is closer to 1, emphasizing the close relationship between the informative index this neuron network displays and the input informational gathering.

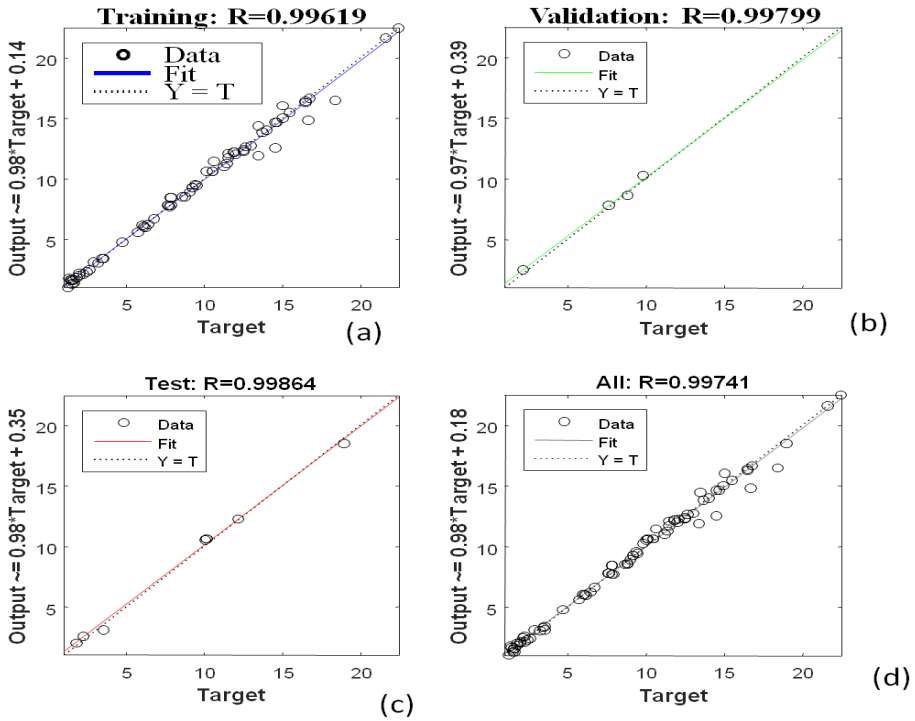

Fig. 6. Modeled data, training datasets, validation datasets, testing datasets, and the input dataset itself were used to fit regression to the input dataset.

By using a direct or nonlinear relapse approach, ANN may determine the relationship between information sources and outcome focuses. For determining the relationship between information sources and results in this situation, the straight relapse approach is used. The seven inputs that this ANN configuration recognizes are the incoming pulse (Pin(t)x1), the width of the incoming pulse ((τ_0)x2), the recovery time of gain of the SOA (τ_e)x3), T_{asym} the loop eccentricity (x4), the control pulse (Pcp(t)x5), the energy of the control pulse(E_{cp}) (x6), and the width of the control pulse(σ) (x7). The outputs are the upper channel (PUpper)[y1] and lower channel (PLower)[y2] (y1 and y2, respectively). The outcome depends on the work we apply to this model. Most of the time, this ability is referred to as actuation work. We have made an effort to address the direct relapse problem with an essential direct condition as our enactment work. As far as a direct capacity, straight relapse is characterized as

$$y_1\text{^}=b_1 + p\text{‘}_1x_1 + p\text{‘}_2x_2 + p\text{‘}_3x_3 + p\text{‘}_4x_4 + p\text{‘}_5x_5 + p\text{‘}_6x_6 + p\text{‘}_7x_7 \quad (3)$$

$$y_2\text{^}=b_2 + p\text{“}_1x_1 + p\text{“}_2x_2 + p\text{“}_3x_3 + p\text{“}_4x_4 + p\text{“}_5x_5 + p\text{“}_6x_6 + p\text{“}_7x_7 \quad (4)$$

where y_1^ and y_2^ are the forecast for the result variable y_1 and y_2 and $x_1,x_2,\ldots,x_7$ are the sources of info, $p_1,p_2,\ldots,p_7$ are the loads and b_1 and b_2 is a predisposition term. With the help of this direct initiation activity, we were able to achieve a 99.74% accuracy rate for this ANN plan. The relationship between unique information, anticipated information, and relapse coefficient is shown in Fig. 6. Figures 5 and 6 reveal that the relapse factor is closer to 1, demonstrating the powerful link between the input informational index and the demonstrated informational index in this neural organization.

V. Results and analysis

The characteristics utilized in this paper were developed based on the writing requirements for numerous research publications [XVI, XVII, XIII]. Several parameters' values, such as: As e is the pickup recuperation time of SOA, the unsaturated enhancer pickup (Gss) of SOA is 20 dB and 100 ps. The Ecp as exchanging beat vitality of 100 fJ and Esat as immersion vitality of the SOA of 1000 fJ are the other characteristics. The few remaining parameters are Tc, which is the bit period, and Tasym, which is the circle's unpredictableness, both measured in pulses per second (ps). The operational requirement was taken into consideration when choosing these criteria. Figures 7 and 8 illustrate the adder, respectively showing the adder circuit's corresponding input and output waveforms.

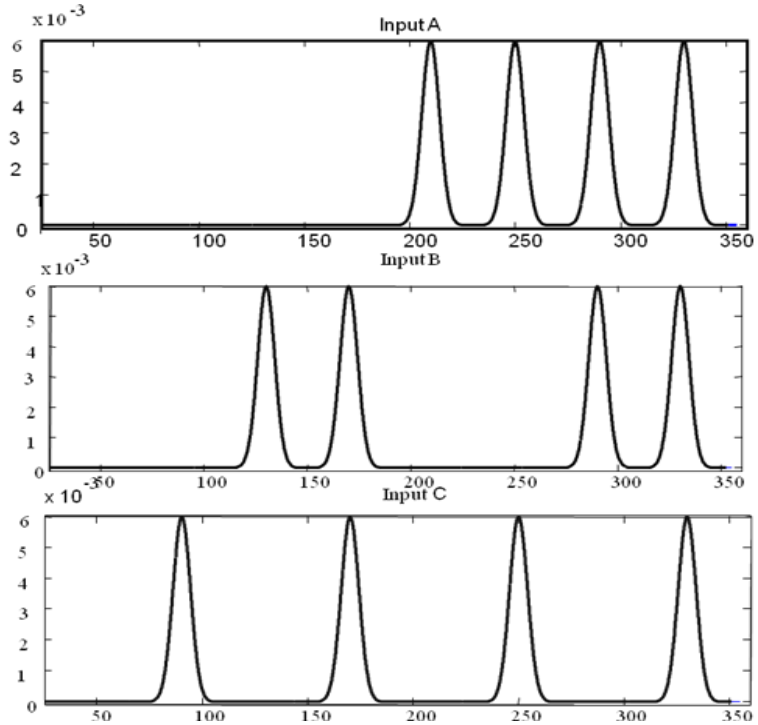

Figure 7: Input waveforms of the Input A and Input B and input C.

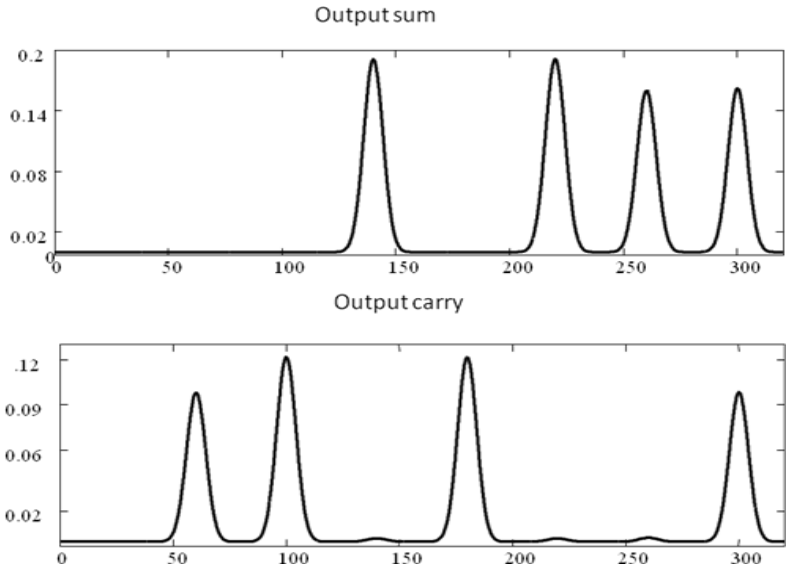

Fig. 7. Output waveforms of the Carry (Cout) and Sum (S).

We witness the proper worth of the SOA short sign increasing when the exchanging power is decreasing, allowing us to focus on the circuit's capacity. As a result, Figure 9 shows how dependent the turning power is on the little sign increase. From this figure,

it can be seen that the power tends to decrease noticeably as the small sign addition increases, reaching at least 100 fJ at 20 dB.

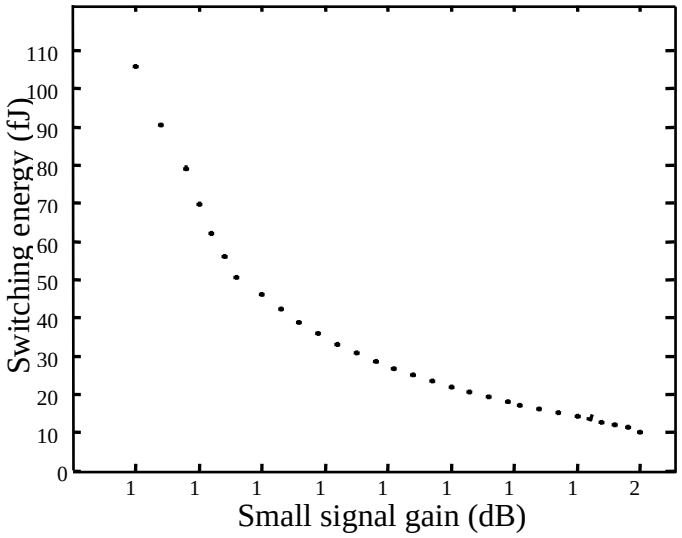

Fig. 8. Switching energy variation with respect to small signal gain.

ER is the extinction ratio. To evaluate our plan, considering the ER as [VII], PO1min stands for the lower power of the 1-state in equation (5). In a similar vein, PO0max is the 0-state's maximum power. ER should preferably be higher than 8.50 dB for better output. Based on the extinction ratio, the 1-state and 0-state can be distinguished from one another rather easily. This design's functionality is reliant on SOA recovery and CP energy.

Figure 10 illustrates how the ER is impacted by the CP's growth, recovery, and energy. It is demonstrated that ER increases with rising CP energy and that it starts to fall off at a particular point (100 fJ and 100 ps). Figure 10 shows that ER is similarly decreased by high expansion recovery durations and CP energy. A dynamic SOA response was obtained to protect against this. Beat demands give it a better chance to regain its fundamental increment over lengthy expansion recovery durations, which lowers ER. When the inundation power is constant, as the gain recovery time goes up, so does the submersion energy. The justification is that less energy is expected to flood the SOA as a result.

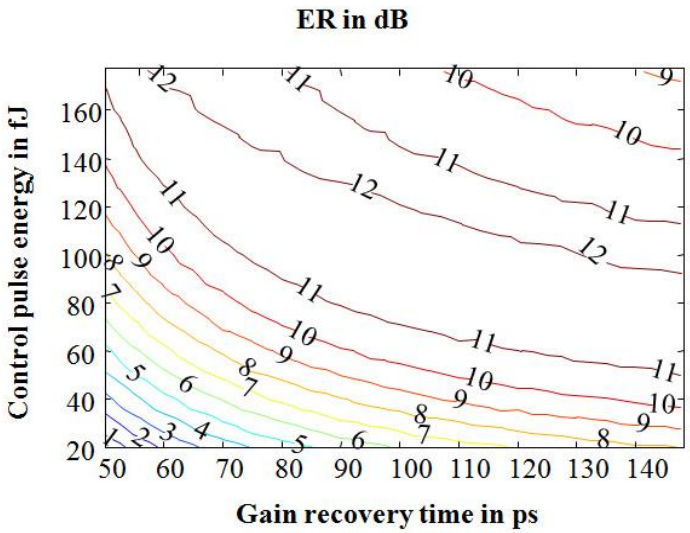

Fig. 9. A variety of ER with increased CP recovery time and energy at the results, while maintaining fixed other boundaries.

One major limitation that has an impact on the circuit display is the optical bit rate component. Gain recovery time and information estimation's effects on the ER are depicted in Figure 11. It claims that lower bit estimation and a longer recovery time lead to a lower ER. This occurs because of a bad method; overall, the SOA needs more to reclaim its advantage and provide the necessary fragment modification. Once a recovery time cost of gain calculation has been made, the ER exhibits consistency. It will require less energy and a smaller bit estimation to attain a given ER.

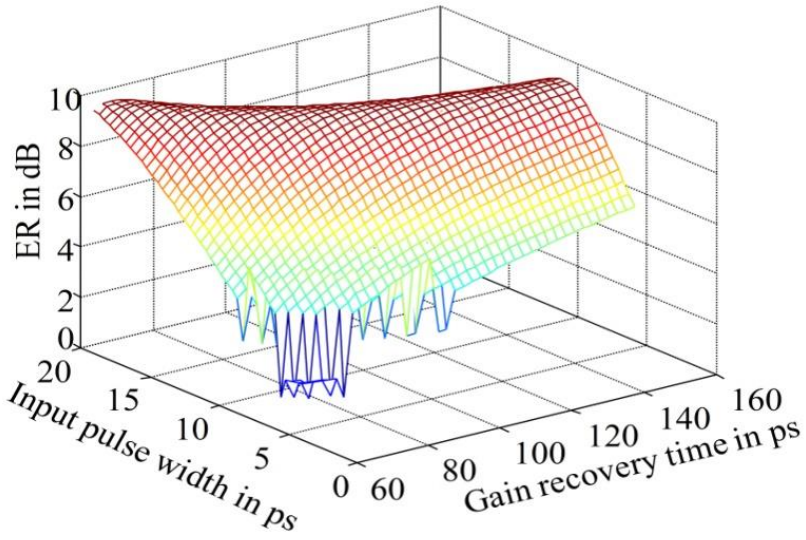

Fig. 10. Shows several ER types with pulse width and recovery duration at the outcomes.

The results are superimposed to create an eye chart when information sources are used more than once, such as when the inputs span from zero to one or one to one, etc. [XV]. Because the locator and optical strands give connection links, like clamour source, that are less illuminating than the deteriorating effects, which are frequently seen in the highlight point, Figure 12 is not a normal eye-outline. A pseudo-eye-chart is what this diagram is called [XXII].

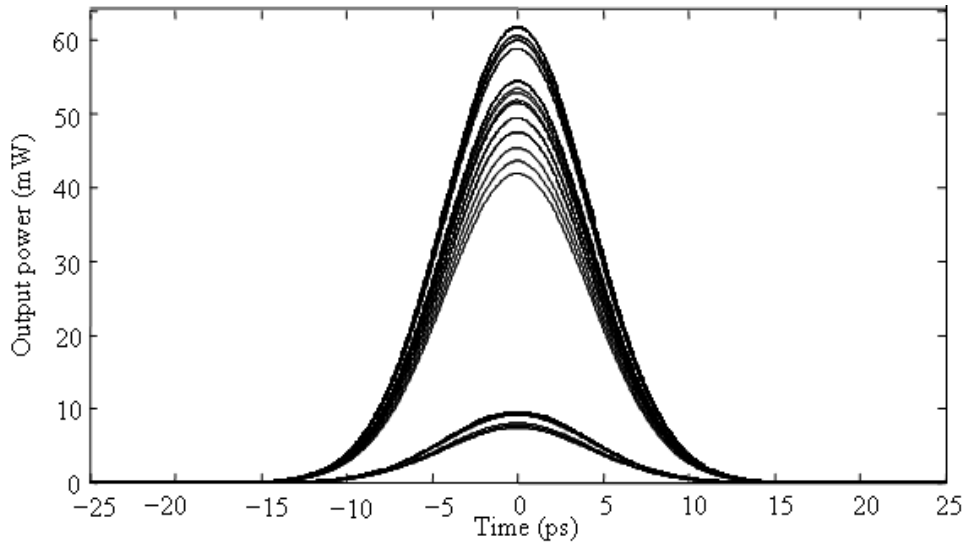

Fig. 11. Pseudo-eye chart.

The most extreme abilities and the base and at 0-state and 1-state, independently, are described as the general eye-opening (O). Huge eyeballs on an eye graph suggest an unambiguous transmission with a low piece rate [IV]. We determine that PED (O) = 87.5 percent. This value shows that the circuit's result terminals have responded reasonably.

VI. Conclusion

Only two TOAD-based switches are used in the optical parallel Full-adder that we designed. The circuit has been theoretically designed and numerically tested. The simulation of the circuit uses both the reflected and transmitted ports. The outputs of this circuit produce the desired outcome. We have designed an ANN-based model of this circuit that is equivalent. Utilizing ANN, this circuit setup has been verified. This optical circuit is effective at arranging light as an input to shape the aim, so it no longer just increases calculation speed. The biggest improvement of this equal circuit is that no synchronization is required for unusual information sources. The ANN model has finished investigating this circuit's subtleties of execution. These circuits can act as the basic building blocks for trickier circuit designs.

Conflict of Interest:

The author declares that there was no conflict of interest regarding this paper.

Reference

I. A. Bhattacharyya, D. K. Gayen, and T. Chattopadhyay, : 'Alternative All-optical Circuit of Binary to BCD Converter Using Terahertz Asymmetric Demultiplexer Based Interferometric Switch.' in *Proceedings of 1st International Conference on Computation and Communication Advancement* (IC3A–2013).

II. A. Poustie, K. J. Blow, A. E. Kelly, and R. J. Manning, : 'All-optical full-adder with bit differential delay.' *Optics Communications* 168 (1-4), 89–93 (1999). 10.1016/S0030-4018(99)00348-X

III. A. Ryou, J. Whitehead, M. Zhelyeznyakov, P. Anderson, C. Keskin, M. Bajcsy, and A. Majumdar, : 'Free-space optical neural network based on thermal atomic nonlinearity.' *Photonics Research* 9 (4), B128–B134 (2021). 10.1364/PRJ.415964

IV. A. Yariv and P. Yeh, : 'Photonics: Optical Electronics in Modern Communications.' *Oxford University Press, UK*, 6th Edition (2007).

V. B. Wang, V. Baby, W. Tong, L. Xu, M. Friedman, R. Runser, I. Glesk, and P. Prucnal, : 'A novel fast optical switch based on two cascaded terahertz optical asymmetric demultiplexers (TOAD).' *Optics Express* 10(1), 15–23 (2002). 10.1364/OE.10.000015

VI. D. K. Gayen, J. N. Roy, C. Taraphdar, and R. K. Pal, : 'All-optical reconfigurable logic operations with the help of terahertz optical asymmetric demultiplexer.' *International Journal for Light and Electron Optics* 122 (8), 711–718 (2011). 10.1016/j.ijleo.2010.04.024

VII. D. K. Gayen, T. Chattopadhyay, M. K. Das, J. N. Roy, and R. K. Pal, : 'All-optical binary to gray code and gray to binary code conversion scheme with the help of semiconductor optical amplifier -assisted sagnac switch.' *IET Circuits, Devices & Systems* 5 (2), 123–131 (2011). 10.1049/iet-cds.2010.0069

VIII. D. K. Gayen, : Optical arithmetic operation using optical demultiplexer. Circuits and Systems.' *Scientific Research*, 7(11), 3485–3493 (2016). 10.4236/cs.2016.711296

IX. D. K. Gayen, 'All-Optical 3:8 Decoder with the Help of Terahertz Optical Asymmetric Demultiplexer.' *Optics and Photonics Journal*, 6 (7), 184–192, July (2016). 10.4236/opj.2016.67020

X. D. K. Gayen, : 'Optical parallel half adder using semiconductor optical amplifier-assisted Sagnac gates.' *Journal of Mechanics of Continua and Mathematical Sciences*, 17 (4), 1-7, April (2022). 10.26782/jmcms.2022.04.00001

XI. H. L. Minh, Z. Ghassemlooy, and W. P. Ng, " 'Characterization and performance analysis of a TOAD switch employing a dual control pulse scheme in high speed OTDM demultiplexer.' *IEEE Communications Letters* 12 (4), 316–318 (2008). 10.1109/LCOMM.2008.061299

XII. J. H. Kim, S. H. Kim, C. W. Son, S. H. Ok, S. J. Kim, J. W. Choi, Y. T. Byun, Y. M. Jhon, S. Lee, D. H. Woo, and S. H. Kim, : 'Realization of all-optical full-adder using cross-gain modulation.' in *Proceedings of the Conference on Semiconductor Lasers and Applications*, SPIE 5628, 333–340 (2005). 10.1117/12.576410

XIII. J. Zhou, B. Huang, Z. Yan and J-C. G. Bünzli, Emerging role of machine learning in light-matter interaction. Light Science & Application 8, 84 (2019). 10.1038/s41377-019-0192-4

XIV. J. P. Sokoloff, P. R. Prucnal, I. Glesk, and M. Kane, : 'A terahertz optical asymmetric demultiplexer (TOAD).' *IEEE Photonics Technology Letters* 5 (7), 787–790 (1993). 10.1109/68.229807

XV. J. Gowar, : 'Optical Communication System.' *Prentice Hall of International Limited, UK*, 2nd Edition (1993).

XVI. K. E. Zoiros, J. Vardakas, T. Houbavlis, and M. Moyssidis, : 'Investigation of SOA-assisted Sagnac recirculating shift register switching characteristics.' *International Journal for Light and Electron Optics* 116 (11), 527–541 (2005). 10.1016/j.ijleo.2005.03.005

XVII. K. E. Zoiros, P. Avramidis, and C. S. Koukourlis, : 'Performance investigation of semiconductor optical amplifier based ultra-fast nonlinear interferometer in nontrivial switching mode.' *Optical Engineering* 47 (11), 115006–11 (2008). 10.1117/1.3028348

XVIII. K. Mukherjee, : 'Method of implementation of frequency encoded all-optical half- adder, half-subtractor, and full-adder based on semiconductor optical amplifiers and add drop multiplexers.' *International Journal for Light and Electron Optics*. 122 (13), 1188–1194 (2011). 10.1016/j.ijleo.2010.07.026

XIX. M Suzuki, H. Uenohara, : 'Invesigation of all-optical error detection circuitusing SOA-MZI based XOR gates at 10 Gbit/s.' *Electron. Lett*, 45 (4), 224–225 (2009). 10.1049/el:20093461

XX. P. Li, D. Huang, X. Zhang, and G. Zhu, : 'Ultra-high speed all-optical half-adder based on four wave mixing in semiconductor optical amplifier.' *Optics Express*, 14 (24), 11839–47 (2006). 10.1364/OE.14.011839

XXI. P. Ghosh, D. Kumbhakar, A. K. Mukherjee, and K. Mukherjee, : 'An all-optical method of implementing a wavelength encoded simultaneous binary full-adder-full-subtractor unit exploiting nonlinear polarization rotation in semiconductor optical amplifier.' *International Journal for Light and Electron Optics* 122 (19), 1757–1763 (2011). 10.1016/j.ijleo.2010.10.039

XXII. Q. Wang, G. Zhu, H. Chen, J. Jaques, J. Leuthold, A. B. Piccirilli, and N. K. Dutta, : 'Study of all-optical XOR using Mach-Zehnder interferometer and differential scheme.' *IEEE Journal of Quantum Electronics* 40 (6), 703–710 (2004). 10.1109/JQE.2004.828261

XXIII. S. Mukhopadhyay and B. Chakraborty, : 'A method of developing optical half- and full-adders using optical phase encoding technique.' in *Proceedings of the Conference on Communications, Photonics, and Exhibition* (ACP), TuX6, 1–2 (2009).

XXIV. T. Wang, S.-Y. Ma, L. G. Wright, T. Onodera, B. C. Richard and P. L. McMahon, : 'An optical neural network using less than 1 photon per multiplication.' *Nature Communications* 13 (123), 1–8 (2022).

XXV. X. Lin, Y. Rivenson, N. T. Yardimci, M. Veli, Y. Luo, M. Jarrahi, and A. Ozcan, : 'All-optical machine learning using diffractive deep neural networks.' *Science*, 361 (6406), 1004–1008 (2018). 10.1126/science.aat8084

XXVI. X. Wu, J. A. Jargon, L. Paraschis and A. E. Willner, : 'ANN-Based Optical Performance Monitoring of QPSK Signals Using Parameters Derived From Balanced-Detected Asynchronous Diagrams.' *IEEE Photonics Technology Letters* 23 (4), 248–250 (2011). 10.1109/LPT.2010.2098025

XXVII. W. Gao, L. Lu, L. Zhou, and J. Chen, : 'Automatic calibration of silicon ring-based optical switch powered by machine learning.' *Opt. Express* 28 (7), 10438–10455 (2020). 10.1364/OE.388931

XVIII. Z. Yu, X. Zhao, S. Yang, H. Chen and M. Chen, : 'Binarized Coherent Optical Receiver Based on Opto-Electronic Neural Network.' *IEEE Journal of Selected Topics in Quantum Electronics* 26 (1), 1–9 (2020). 10.1109/JSTQE.2019.2931251